Advances in Aircraft and Spacecraft Science, *Vol. 11, No. 4 (2024) 331-361*
https://doi.org/10.12989/aas.2024.11.4.331

Impact response of bio-inspired curved laminated composite plates: A numerical simulation

Faisal K. Baakeel[1], Mohamed A. Eltaher*[1,2] and Muhammad A. Basha[1]

[1]*Mechanical Engineering Department, Faculty of Engineering, King Abdulaziz University, Jeddah, Saudi Arabia*
[2]*Mechanical Design and Production Department, Faculty of Engineering, Zagazig University, Egypt*

(Received December 12, 2023, Revised January 14, 2025, Accepted January 15, 2025)

Abstract. This study aims to develop a numerical simulation model that investigates the load response of the low velocity impact for curved plates with different layup configurations using unidirectional carbon fiber-reinforced polymer (CFRP). At first, the commercial explicit finite element code LS-DYNA is used to develop the numerical simulation model to validate the experimental finding of a published work. A 2D modeling approach with a single shell element is adopted. The plies thickness and fiber orientations are defined using PART_COMPOSITE. The elasto-plastic composite material model MAT54, based on the failure criteria, is used to define the unidirectional composite material, while MAT20 is used to define the impactor material as a rigid body. The numerical simulation results show a strong agreement with the experimental results in terms of absorbed energy, impact force, and deflection plots. Consequently, the developed model is used to study the impact response and resistance of different curved plates (R0 (Flate), R500, R750, and R1500), and different layup configurations (Unidirectional (UD), Cross-Ply (CP), Quasi-Isotropic (QI), Linear bio-inspired Helicoidal (LH), and nonlinear bio-inspired Fibonacci-Helicoidal (FH)). The designed CFRP plate consist of 32-plies with overall dimensions of 300×150×3.6 mm. The CFRP plate is impacted by a hemispherical steel impactor of 25.4 mm diameter and 6.5 m/s speed to generate 40 J of impact energy. Each layup configuration is analyzed separately with different plate curvatures to discover the advantages of the curved plates over the flat plate in order to improve the low velocity impact resistance. The curved plates showed excellent behavior in reducing the impact force and deflection during the low velocity impact simulation for all layup configurations. It can be concluded from this study that the curved plates can be effective in enhancing structural impact resistance under low velocity impact conditions, while the following numerical simulation model can be effectively utilized for the purpose of designing and analyzing innovative bio-inspired composite structures in various configurations under different impact scenarios to study the load response.

Keywords: bio-inspired; composite structures; curved plates; low velocity impact; LS-DYNA®; simulation

1. Introduction

During operations, the composite structures are subjected to impact, although there are many advantages of using laminated composite structures instead of metals, there are some disadvantages that laminate composite structures can be exposed to when impacted, including; delamination, matrix cracking, reduced stiffness, reduced fatigue life, and repair difficulty. The

*Corresponding author, Professor, E-mail: meltaher@kau.edu.sa, mohaeltaher@gmail.com

http://www.techno-press.org/?journal=aas&subpage=7 ISSN: 2287-528X (Print), 2287-5271 (Online)

low velocity impact produces global structure deformation and hidden internal damage at locations far from the contact region because of the long contact time between the impactor and target (Maamar and Ramdane 2016). The low velocity impacts are dangerous for composite structures because they can generate Barely Visible Impact Damage (BVID), which can lead to large drops in the strength and stability of the structures.

Curved composite structures are utilized in several engineering fields due to their significant capacity to carry external loads, attributed to the curvature effect on shells. The extensive utilization of laminated composite shells can be associated with their superior strength and stiffness-to-weight ratios in comparison to most metallic materials. Nowadays, laminated composite shells represent a major proportion of aerospace, automotive, and marine structures. In addition to meeting geometrical constraints, changing the laminated composite shells from a flat to a curved shape can significantly enhance the impact response in a variety of composite applications. However, impact analysis studies primarily focus on the impact performance of flat plates or cylinder specimens. The primary investigation of the low-velocity impact behavior of curved composite structures was conducted by the researchers using several cylindrical curved specimens (Kim *et al.* 1997, Krishnamurthy *et al.* 2003, Saghafi *et al.* 2014). Therefore, the comprehensive knowledge of the deformation and damage characteristics of curved structures is crucial for transferring the analyzed impact behavior of flat specimens to general curved structures, which optimizes the lightweight capability of a load-specific structure (Gebhardt *et al.* 2023). Generally, the curved plates can be examined to control the impact behaviors in terms of energy absorption, impact force, deformation, and consequently the resulted intra-laminar and inter-laminar damages.

Bio-inspiration is the creation of unique materials and structures that are motivated by solutions discovered through the millions of years of biological evolution and improvement (Sanchez *et al.* 2005). Because their potential for use in bio-inspired composites has been explored, researchers have examined a variety of biological artifacts. Evidently, it will be useful to study the creatures with naturally formed armours as it can lead to inspiration and novel design of synthetic structures mimicking the advanced mechanical architectures of their natural creatures. The helicoidal arrangement present in various creatures as a naturally strong defense armour, is a particular interesting feature, which is one of the main subjects of this study. The bio-inspired composite structures with helicoidal schemes have high impact energy absorption capability, which can enhance the impact resistance of the composite structures.

Finite element software provides a comprehensive platform for the simulation and analysis of the impact response of composite materials. Bhaskar and Thakur (2019) studied the nonlinear behavior of the laminated composite plates under transverse sinusoidal loading using a new inverse trigonometric shear deformation theory by finite element method. Alessi *et al.* (2023) studied the dynamic analysis of piezoelectric perforated cantilever bimorph energy harvester via finite element analysis. Baakeel *et al.* (2023), studied Static and modal analysis of bio-inspired laminated composite shells using numerical simulation. Rachid *et al.* (2018) presented theoretical and numerical study on the behavior of a tapered shaft rotor made of composite materials by the classical version h and the version p of the finite element method. Through the use of sophisticated material models, accurate meshing methods, and suitable contact modeling, scientists are able to acquire significant knowledge on the response of composite structures when subjected to impact loading. The modeling and simulation of composite materials became more interesting, where it is possible to numerically adjust the number of layers, fiber orientation, or curvature angle with ease, compared with the practical experiments, which eventually will be more expensive and may

require custom fabrication.

Numerous review articles that describe the research on the analysis of laminated composite plates and shells under low velocity impact and various loading circumstances related to this study can be found in the literature. Several studies on the failure nature characteristics of fiber-reinforced composites under impact loading have been carried out in recent years (de Vasconcellos *et al.* 2014, Caprino *et al.* 2015, Liang *et al.* 2015, Thomason *et al.* 2018, Ahmed *et al.* 2021, Jayatilake *et al.* 2015, Kaci *et al.* 2016). Several researchers have conducted experimental work to investigate the complicated behavior of laminated composite plates when subjected to impact loading (Sayer *et al.* 2010, Atas *et al.* 2011, Jordan *et al.* 2013, Kurşun *et al.* 2015, Ying *et al.* 2016, Miao *et al.* 2019, Fuga *et al.* 2021, Seifoori *et al.* 2021, Kravchenko *et al.* 2021). The impact behavior of complex composite materials can be simulated by utilizing the constitutive models as outlined in the references (Faggiani *et al.* 2010, Iannucci *et al.* 2006, Lapczyk *et al.* 2007, Metoui *et al.* 2018, Donadon *et al.* 2008, Baakeel *et al.* 2025).

Among the several advanced numerical techniques, the progressive damage model (PDM) has been considered as the most popular modeling scheme that considers the initiation of damage and the subsequent degradation of stiffness (Donadon *et al.* 2008, Tay *et al.* 2008, Liu *et al.* 2016, Zhang *et al.* 2015, Guo-dong *et al.* 2009, Lee *et al.* 2015). Regarding the evaluation of damage initiation in composites, many interaction criteria using distinct expressions to evaluate fiber and matrix damage under tensile and compression loading have been widely used, including Hashin (Hashin *et al.* 1973, 1980, Chang-Chang 1987, Hou 2000, 2001) criteria. Once the failure criterion is met, an appropriate damage evolution model needs to be proposed to properly describe the loss of stiffness. Some researchers simulated the process of damage accumulation around the damaged area using the predefined constants for the stiffness degradation rule (Zhang and Zhang 2015a, b), where this approach is not suitable for a wide range of composite simulations. The equivalent displacement approach in damage evolution models is currently used by researchers to predict the progressive damage behavior of composite materials as it involves mechanical factors (Liu *et al.* 2016, Zhang *et al.* 2015, Guo-dong *et al.* 2009).

The analysis of interlaminar crack propagation using finite element techniques such as the Virtual Crack Closure method (VCC) or Cohesive Zone Models (CZM) is now widely being performed using fracture mechanics (Wisnom 2010, Tay 2003, Camanho 2003). The VCC technique is very sensitive to mesh geometry and density, where it must assume that a crack already exists and use adaptive re-meshing techniques to adjust the mesh to the changing shape of the delamination front. The CZM technique combines the strength-based criteria to predict damage initiation with the fracture mechanics energy criteria to simulate damage propagation and the subsequent fracture. Thus, the main limitations of VCC analyses can be overcome, and cohesive interface elements have gained particular interest for the simulation of discrete failure modes in impacted composite laminates. The cohesive elements set at the contact between layers have been used in various studies to simulate the delamination phenomena of composite laminates caused by low-velocity impacts (Aymerich *et al.* 2009, Amaro *et al.* 2011). In further studies, the combined impact of intralaminar and interlaminar damage was examined. The cohesive elements (de Moura 2004, Zhang *et al.* 2006, Aoki 2007, Aymerich *et al.* 2008) and the special spring elements (Bouvet *et al.* 2009, 2012) were used to model the development of major matrix cracks (such as bending cracks on the bottom layer and shear matrix cracks in the middle layers) as well as delamination at the interfaces between layers in impacted laminates.

The significance of this study is to address the improvement and outstanding ability of curved composite plates, with the aim of investigating the bio-inspired helicoidal layup. In this study, a

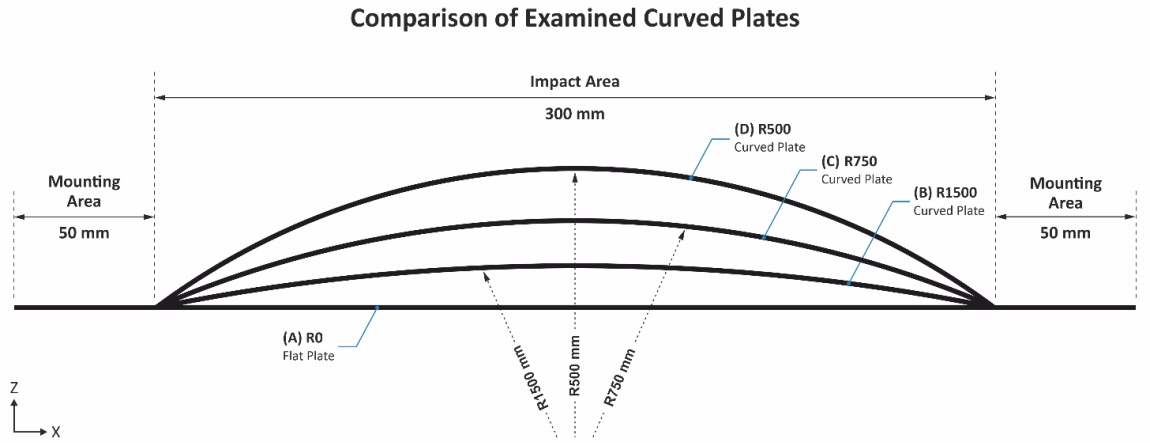

Fig. 1 Side view of different curved plates examined in this study

numerical simulation model was developed using the commercial explicit finite element code LS-DYNA to validate the results of a published experimental work by Heimbs *et al.* (2009). The main purpose of the validation model is to ensure that the developed model is correct and the results are matching with the experimental findings in terms of impact force, absorbed energy, and deflection. Based on the developed numerical simulation model, different curved plates and layup configurations have been considered to investigate the impact load response. The curved radii in mm include the following: R0 (Flate), R500, R750, and R1500. The layup configurations include the following: Unidirectional (UD), Cross-Ply (CP), Quasi-Isotropic (QI), linear bio-inspired, known as Linear-Helicoidal 24° (LH), and non-linear bio-inspired known as Fibonacci-Helicoidal (FH).

2. Curved plates

In this study, different curved plates were examined to investigate the effects of the curvature angle on the impact load response. The curved radii in mm include the following (as shown in Fig. 1):

(A) R0 [Flate Plate]
(B) R1500 [Curved Plate]
(C) R750 [Curved Plate]
(D) R500 [Curved Plate]

The design of the curved laminated composite structures is essential to enhancing the structure's responses to impact loads to effectively utilize the composites lightweight potential. The R0 is an indication reference for the general flat plate. The other curved plates are tested with a specific increase in radius size. The curved plates are chosen to be positive angles after making different trials with the negative angles, which indicates that the CFRP plates with
the positive angles were better in impact resistance in terms of impacted force and resulted damage observed during impact simulation.

The size of the designed plates is considered based on the specified experimental work that will be detailed in the following topics. The main purpose is to modify the curvature of the impacted

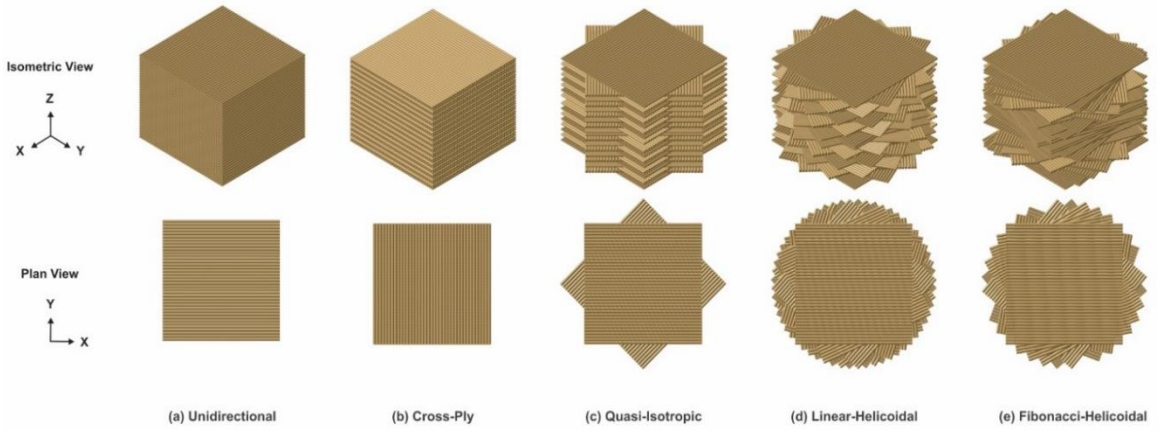

Fig. 2 Different layup configurations examined in this study

area. An extension of 50 mm from each side is considered to simulate real impact specimens, which can be manufactured easily with applicable forming molds. It's well known that the curved plates will have a larger length than the flat plates (i.e., more than 300 mm) and hence more impact surface, while the projected distance will be fixed at 300 mm.

3. Bio-inspired Helicoidal configurations

In this study, different layup configurations were examined to investigate the effects of fiber orientation on the impact load response. These configurations include: Unidirectional (UD), Cross-Ply (CP), Quasi-Isotropic (QI), linear bio-inspired known as Linear-Helicoidal 24° (LH) (Wang *et al.* 2021), and non-linear bio-inspired known as Fibonacci-Helicoidal (FH) (Mohamed *et al.* 2022, Mohamed *et al.* 2023, Karamanli *et al.* 2024), as shown in Fig. 2.

The UD layup is considered as a simple unidirectional (0°) orientation in the longitudinal side of the plate. The CP layup consists of plies arranged in an alternating orthogonal (0°/90°) orientation, which considered to be an effective layout for the penetration resistance. The QI layup the most familiar stacking sequence of plies (0°/45°/90°/-45°), and its properties refer to the in-plane isotropic characteristics that can be achieved in laminates by arranging the fibers in multiple directions, to maintain similar properties when the laminate is loaded in-plane, in flexure, compression or tension, on any axis. The helicoidal structure observed in the endocuticle of the mantis shrimp's dactyl club provides the basis inspiration for the development of helicoidal layup configuration of the composite plies. The LH layup consists of stacking plies with a linear constant rotation angle of 24° (0°/24°/48°/…/360°), which is the angle difference refers to the variation in orientation between adjacent layers. The FH layup is designed as a non-linear helicoidal plies based on the Fibonacci sequence starting from 0° and 10°, where the angle of each following ply is the sum of the two preceding ones (0°/10°/10°/20°/…/340°). The specifications of the different layup configurations are presented in Table 1.

4. Validation FEM model for an experimental testing

Table 1 Specifications of the different layup configurations, Wang *et al.* (2021)

Designation	Stacking Sequence
(1) UD	Unidirectional - Symmetric $[0^{\circ}/0^{\circ}/0^{\circ}/0^{\circ}/0^{\circ}/0^{\circ}/0^{\circ}/0^{\circ}/0^{\circ}/0^{\circ}/0^{\circ}/0^{\circ}/0^{\circ}/0^{\circ}/0^{\circ}/0^{\circ}/0^{\circ}]_s$
(2) CP	Cross-Ply - Symmetric $[0^{\circ}/90^{\circ}/0^{\circ}/90^{\circ}/0^{\circ}/90^{\circ}/0^{\circ}/90^{\circ}/0^{\circ}/90^{\circ}/0^{\circ}/90^{\circ}/0^{\circ}/90^{\circ}/0^{\circ}/90^{\circ}]_s$
(3) QI	Quasi-Isotropic - Symmetric $[0^{\circ}/45^{\circ}/90^{\circ}/-45^{\circ}/0^{\circ}/45^{\circ}/90^{\circ}/-45^{\circ}/0^{\circ}/45^{\circ}/90^{\circ}/-45^{\circ}/0^{\circ}/45^{\circ}/90^{\circ}/-45^{\circ}]_s$
(4) LH	Linear-Helicoidal (24°) - Symmetric $[0^{\circ}/24^{\circ}/48^{\circ}/72^{\circ}/96^{\circ}/120^{\circ}/144^{\circ}/168^{\circ}/192^{\circ}/216^{\circ}/240^{\circ}/264^{\circ}/288^{\circ}/312^{\circ}/336^{\circ}/360^{\circ}]_s$
(5) FH	Fibonacci-Helicoidal - ($F_n = F_{n-1} + F_{n-2}, F_0 = 0, F_1 = 10$) - Symmetric $[0^{\circ}/10^{\circ}/10^{\circ}/20^{\circ}/30^{\circ}/50^{\circ}/80^{\circ}/130^{\circ}/210^{\circ}/340^{\circ}/190^{\circ}/170^{\circ}/360^{\circ}/170^{\circ}/170^{\circ}/340^{\circ}]_s$

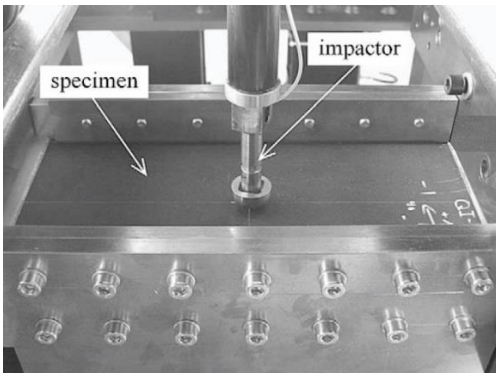

Fig. 3 Fixture design and experimental setup view (Heimbs *et al.* 2009)

The main purpose of the validation model is to ensure that the developed model is correct, and the results are matching with the experimental findings in terms of impact force, absorbed energy, and deflection. This will provide confidence to the results and findings when the curved plates and bio-inspired layup were applied.

Therefore, the low velocity impact testing (developed by Heimbs *et al.* 2009) was conducted on a Dynatup 8250 drop tower, will be used to develop the validation model. The experimental case, designated as Type-B (prepreg) 40 J unloaded, was the main focus of the study. The mounting fixture design and the experimental testing setup are illustrated in Fig. 3.

The detailed validation model will be published in another paper, while the main topics are summarized as follows.

4.1 Low velocity impact testing (Benchmark)

A hemispherical steel impactor with 1.0-inch (25.4 mm) diameter and 1.85 kg of mass was used for the low velocity impact testing. The impact velocity was 6.5 m/s resulting an energy level of 40 J. The CFRP specimens were clamped under conditions that included a fixed support for the longitudinal ends and a simple support for the lateral sides.

Table 2 Lamina elastic and strength properties (Heimbs *et al.* 2009)

Material	12K HTS/ 977-2
ρ [kg/m^3]	1620
E_{11} [GPa]	153
E_{22} [GPa]	10.3
G_{12} [GPa]	5.2
ν_{12}	0.3
σ_{11}^{+} [MPa]	2540
σ_{11}^{-} [MPa]	1500
σ_{22}^{+} [MPa]	82
σ_{22}^{-} [MPa]	236
τ_{12} [MPa]	90

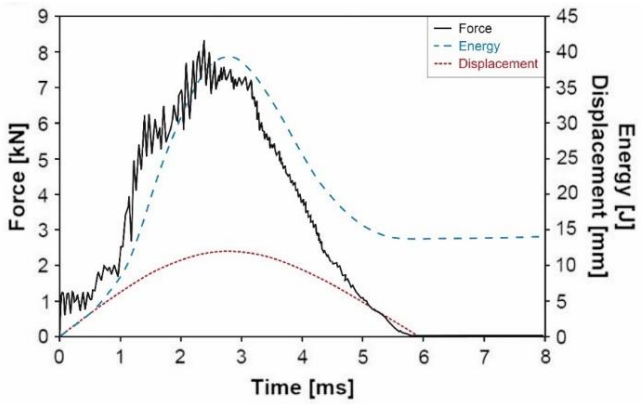

Fig. 4 Experimental results of force, energy and displacement (Heimbs *et al.* 2009)

4.2 Testing material (Benchmark)

The material used in the experiment was prepreg material from the manufacturer Cytec. The 12K HTS unidirectional carbon fibers were already pre-impregnated with 977-2 epoxy matrix to produce a symmetric quasi-isotropic plate consists of 24 plies: $[-45^{\circ}/0^{\circ}/45/90^{\circ}]_{3s}$. The average thickness of the cured plate was 2.7 mm. Table 2 present the lamina elastic and strength material properties. The CFRP material was prepared into test specimens of 400 mm length and 150 mm width. On both sides of the specimens, double-tapered GFRP tabs of 2 mm thick and 50 mm wide were bonded. This reduced the free length of the specimen to 300 mm.

4.3 Experiment results (Benchmark)

Fig. 4 shows the experimental results of the impact testing for the unloaded CFRP plates in terms of time-dependent plots of impact force, energy absorption, and deflection. The energy was computed using the initial kinetic energy, mass, and velocity of the impactor. A photoelectric sensor was used to measure the initial velocity before impact.

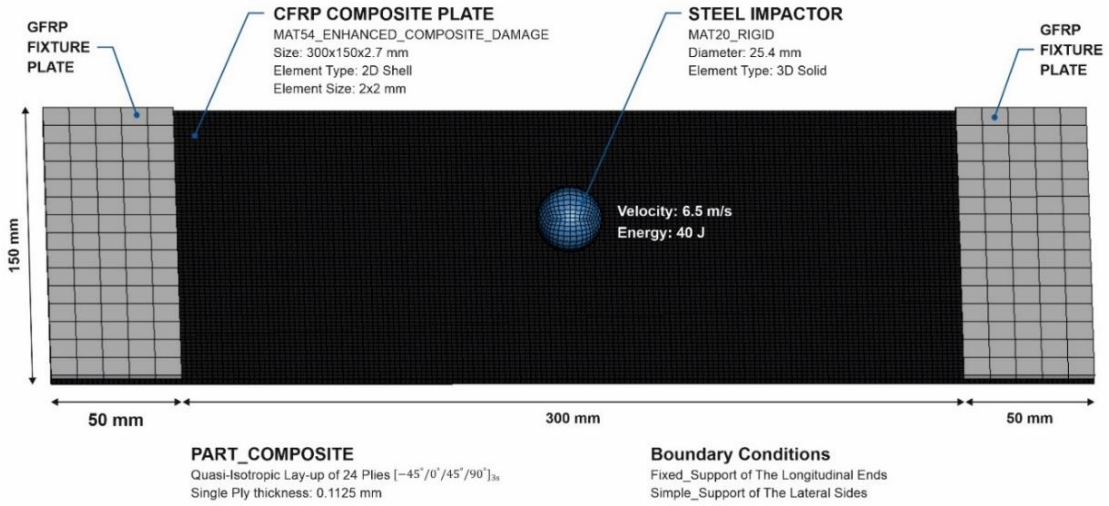

Fig. 5 Layout of the numerical simulation model

4.4 Numerical simulation modeling

The numerical model of the low velocity impact simulation was developed using the commercial explicit finite element code LS-DYNA and involves modeling both the composite plate and the rigid impactor with appropriate contact definitions. The layout of the numerical simulation model is illustrated in Fig. 5. The modelling topics are addressed as follows.

4.5 Composite plate modeling

The most critical part of this simulation model is the modeling of the CFRP composite plate due to its complexity. Although the thin composite structure has a large aspect ratio compared to the laminate thickness, it implies that the structural system is globally three-dimensional. Consequently, it is common to use 2D shell elements, where each layer can be assumed to be in a state of plane stress. Therefore, the CFRP plate was modeled as 2D shell of 400×150 mm size, using the Shape_Mesher and the 4N_Shell Entity. The 4-node shell element size was 2 mm, to balance the simulation's accuracy and efficiency. The shell element formulation was defined using the default option; Belytschko-Tsay (ELFORM 2) which has 6 degrees of freedom at each node.

In this model, the linear elastic-plastic model MAT_ENHANCED_COMPOSITE_DAMAGE (MAT54) based on the failure criteria by Chang and Chang (1987) was used to define the composite material properties. This progressive failure model was created specifically to deal with various orthotropic materials like unidirectional composite laminates.

MAT54 consists of 63 input parameters arranged in a matrix of 9 rows and 8 columns, where each row represents a card. The values of these cards mainly represent the material model, which includes the elastic orthotropic material parameters for the longitudinal, transverse and normal direction, the material coordinate system that defines the material direction to control the anisotropic behavior, the failure modeling parameters, the strain parameters and nonphysical parameters that ensure the element is retained after the failure criterion is met and is not removed until the failure strain is exceeded, the strength limits of the Chang-Chang or Tsai-Wu failure

criterion, and some additional tuning parameters to control the simulation.

The elastic input constants of the MAT54 are defined using the Young's moduli (EA, EB, EC), the Poisson's ratios (PRBA, PRCA, PRCB) and the shear moduli (GAB, GBC, GCA). Each ply in the laminate will be considered as an integration point in the two-dimensional element when the laminated material is simulated. In the elastic region, Chang and Chang (1987) theory will be applied to the material stress-strain relations. The elastic stress-strain relations in each ply are given by:

I. For fiber (axial, 1-direction)

$$\varepsilon_{11} = \frac{1}{E_1}(\sigma_{11} - \nu_{12}\sigma_{22}), \tag{1}$$

II. For matrix (transverse, 2-direction)

$$\varepsilon_{22} = \frac{1}{E_2}(\sigma_{22} - \nu_{12}\sigma_{11}), \tag{2}$$

III. For shear (12-direction)

$$2\varepsilon_{12} = \frac{1}{G_{12}}\sigma_{12} + \alpha{\sigma_{12}}^3, \tag{3}$$

The nonlinear shear stress-strain relation developed by Hahn and Tsai (1973) will be used. Where the term α is the weighting factor for the nonlinear shear stress term. The term α is an input parameter in MAT54 (defined as ALPH), which required calibration through trial and error because it cannot be determined experimentally.

In the plastic region, MAT54 apply the failure criteria developed by Hashin (1980), who specified four distinct failure modes for the unidirectional laminated composite under plane stress, whereas Chang and Chang only specify the two failure modes (fiber and matrix). The four failure criteria are represented in the history variables of MAT54, and they are given as follows:

I. For the tensile fiber mode where $\sigma_{11} \geq 0$:

$$\begin{gathered} e_f^2 = \left(\frac{\sigma_{11}}{X_t}\right)^2 + \beta\left(\frac{\sigma_{12}}{S_c}\right)^2 - 1, \\ e_f^2 \geq 0 \implies \text{failed} \\ e_f^2 < 0 \implies \text{elastic} \\ \text{On failure: } E_1 = E_2 = G_{12} = \nu_{21} = \nu_{12} = 0 \end{gathered} \tag{4}$$

II. For the compressive fiber mode where $\sigma_{11} < 0$:

$$\begin{gathered} e_c^2 = \left(\frac{\sigma_{11}}{X_c}\right)^2 - 1, \\ e_c^2 \geq 0 \implies \text{failed} \\ e_c^2 < 0 \implies \text{elastic} \\ \text{On failure: } E_1 = \nu_{21} = \nu_{12} = 0 \end{gathered} \tag{5}$$

III. For the tensile matrix mode $\sigma_{22} \geq 0$:

$$e_m^2 = \left(\frac{\sigma_{22}}{Y_t}\right)^2 + \left(\frac{\sigma_{12}}{S_c}\right)^2 - 1,$$

$$\begin{gathered} e_m^2 \geq 0 \implies \text{failed} \\ e_m^2 < 0 \implies \text{elastic} \\ \text{On failure: } E_2 = \nu_{21} = G_{12} = 0 \end{gathered} \tag{6}$$

IV. For the compressive matrix mode where $\sigma_{22} < 0$:

$$\begin{gathered} e_d^2 = \left(\frac{\sigma_{22}}{2S_c}\right)^2 + \left[\left(\frac{Y_c}{2S_c}\right)^2 - 1\right]\frac{\sigma_{22}}{Y_c} + \left(\frac{\sigma_{12}}{S_c}\right)^2 - 1, \\ e_d^2 \geq 0 \implies \text{failed} \\ e_d^2 < 0 \implies \text{elastic} \\ \text{On failure: } E_2 = \nu_{21} = \nu_{12} = G_{12} = 0 \end{gathered} \tag{7}$$

The specified elastic properties for a given ply within the element are set to zero when one of the above conditions is exceeded. Where the term β is the shear stress weighting factor. The term β is an input parameter in MAT54 (defined as BETA) that allows the user to specify exactly how shear will affect the tensile fiber mode. When $\beta = 1$, the original criterion of Hashin in the tensile fiber mode is implemented, and when $\beta = 0$, the maximum stress criterion is applied. The BETA value can be chosen based on matter of preference or by trial and error (Wade *et al.* 2012). The LS-Dyna documentation preferers using $\beta = 0$ (the default value in MAT54), which is found to be better compared to experiments (LS-DYNA 2007). In this model, BETA value set to 0. Therefore, the Chang\Chang failure criterion will be applied.

MAT54 can also describe the material's deformation resistance after failure using the SLIM parameters, which is particularly important for compressive failure modes. When the strain values reached specific DFAILX, the element will be removed from the model. SLIM parameters built to account for one structural response, that is the residual of the residual strength of the materials after failure. In addition to the ideal plastic behavior a residual stress can be defined in all directions: the fiber tension (SLIMT1), matrix tension (SLIMT2), the fiber compression (SLIMC1), the matrix compression (SLIMC2) and the shear stress (SLIMS). At the point of failure, the stress level will drop to the residual stress level instead of remaining at its highest level (i.e., a SLIMT1 value of 0.4 will stop the stress dropping below 40% of the ultimate tensile stress).

SLIM parameters are considered as non-physical parameters and should be calibrated by comparing the simulation results with experimental findings (Zhou *et al.* 2018). In this model, SLIM parameters were set to the recommendation values in the LS-Dyna material documentation for MAT58 (MAT_LAMINATED_COMPOSITE_FABRIC).

SOFT parameter is a strength reduction factor that allows for greater stability in crashfront element simulation (Feraboli *et al.* 2011). SOFT parameter is used for softening the load transition from the active row of elements to the next by reducing the strength of the elements immediately ahead of the crushfront to simulate damage propagation and achieve stable and progressive crushing. The crashfront elements are those that share nodes with a deleted element and can have their strengths reduced by using the SOFT parameter, where TFAIL (time step size criteria for element deletion) must be greater than zero to activate this option. Approaching failure, the load in the active row of elements reaches its maximum value, and at failure, it suddenly drops to zero. The strength reduction is applied to the material strengths using the following equation:

$$\{\mathrm{XT}, \mathrm{XC}, \mathrm{YT}, \mathrm{YC}\} = \mathrm{SOFT} * \{\mathrm{XT}, \mathrm{XC}, \mathrm{YT}, \mathrm{YC}\}^*, \tag{8}$$

where the asterisk $(*)$ indicates the pristine strength value.

Feraboli *et al.* (2011), have listed various options for the choice of SOFT parameters in crash front element simulation as follows:

- If $\mathrm{SOFT} = 1$ (default), this indicates that elements at the crush front retain their pristine strength and no softening occurs.
- If $\mathrm{SOFT} = 0$, this sudden transition may lead to unstable buckling of the section (SOFT is inactive).
- If $\mathrm{SOFT} \approx 0$ (close to zero), this will result in a nearly complete loss of strength.
- If $\mathrm{SOFT} > 1$, the model acts as if SOFT set to 0 (SOFT is inactive).

However, setting the SOFT value is a critical issue in the impact simulation because this parameter requires calibration through trial and cannot be determined experimentally (Feraboli *et al.* 2011). Therefore, an attention effort was paid to investigate the effect of this parameter. Finally, the SOFT value is calibrated to 1.8 after many trials.

In MAT54, ply stress exceeding the specified DFAIL parameter results in an immediate reduction of ply stresses to zero. Once all layers reach the zero-stress value, the element is deleted. Therefore, the DFAIL parameters have a direct influence on the deletion of MAT54 elements [50]. When an element undergoes a severe distortion that requires a very small-time step, it may also result in the deletion of the element. The minimal time step parameter, defined as TFAIL (Time step size criterion for element elimination), is

- If $\mathrm{TFAIL} \leq 0$, No element deletion by time step
- If $0 < \mathrm{TFAIL} \leq 0.1$, Element is deleted when its time step is smaller than TFAIL
- If $\mathrm{TFAIL} > 0.1$, Element is deleted when the following conditions happened: $\frac{\text{Actual time step}}{\text{Original time step}} < \mathrm{TFAIL}$

Defining TFAIL close to the element time step would cause premature element deletion since the element would violate the TFAIL condition near its initial state. Also, it is not recommended to depend on element deletion caused by a time-step limitation as the primary source of element deletion, since this is only a computational function that may lower the computational cost of a severely distorted simulation (Wade *et al.* 2012). In this model, TFAIL value is set to a very small and non-zero time step of 1e-7 seconds, which is a preferred value used by many researchers (Feraboli *et al.* 2011, Zhou *et al.* 2018, Cherniaev *et al.* 2018).

When using multi-layers composites with different characteristics, one layer could fail before another, although the material has partially failed, it can still withstand more stress until all of the layers fail. The failure behavior of composites in numerical simulation is one of the main differences between single-layer and multi-layer definition.

Using MAT54, it is possible to determine the percentage of layers that must fail to remove the shell element from the system using the parameter PFL (Percentage of layers which must fail before crashfront is initiated). The default value of PFL is 100, i.e., all layers must fail to remove the element. To simulate the lamina impact in reality, the estimated value of PFL in this model is set to 70.

Consistency in a numerical simulation is achieved when the derived quantities, such as force, stress, and energy, are expressed correctly in terms of the base units (mass, length, and time). The base units used in this model are mass in kilograms (kg), length in meters (m), and time in seconds (s), which result in the derived quantities as follows: force in Newtons (N), stress in Pascals (Pa), energy in Joules (J), velocity in meters per second (m/s), and density in kg per cubic meter (kg/m^3). The main input parameters that describe the CFRP material properties in MAT54 are presented in Table 3.

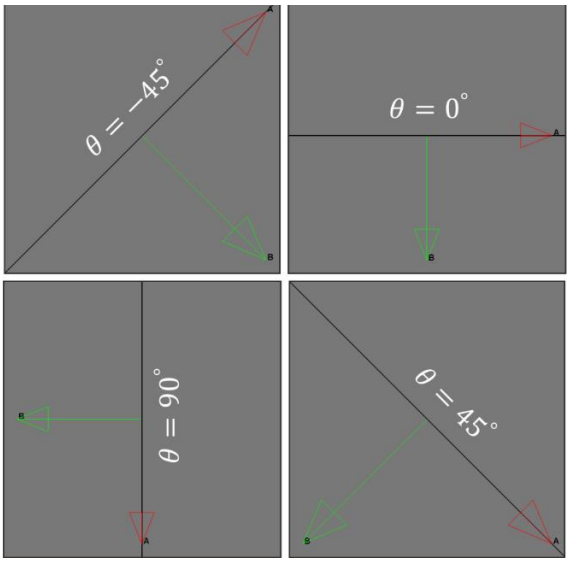

Fig. 6 Illustration of the quasi-isotropic fiber orientations ($-45^{\circ}/0^{\circ}/45/90^{\circ}$) for an element using LS-Dyna *PART_COMPOSITE feature

When conducting FEA to model a composite laminate, there are two main approaches. The first approach is to combine all the plies into a single shell element by summing the properties of each lamina. In the second method, distinct element layers are used to simulate each ply individually, and these layers are then joined using a cohesive element or a contact condition. Considering the first approach when modeling a laminate with only a single shell element, each lamina has its own integration point through the thickness so that the stress state in each ply can be captured. Although this approach has a low computational cost, it does not capture the interlaminar failures such as delamination phenomena.

PART_COMPOSITE feature in LS-Dyna provides a simple way to define a laminated composite into shell elements. PART_COMPOSITE allows to assign different material properties, fiber orientation, and variable thickness within one layer of multiple integration points. This card combines both the SECTION_SHELL and the PART card into one master card. PART_COMPOSITE is used in this model to define the 24 layers of the quasi-isotropic layup, where each layer was 0.1125 mm thick, giving the laminate a total thickness of 2.7 mm. The standard shell element formulation of Belytschko-Tsay (ELFORM 2) with only one point integration is used. Hence, once all integration points of the shell element fail, the element will be deleted, i.e., removed from the calculation. Elements that have common nodes with the deleted element are referred as “crashfront” elements, and their strengths will be reduced by using the SOFT parameter.

The total thickness of the shell can be checked using the thickness appearance option (Appearance→ Thick), while the fiber orientation of an element in any layer within the shell can be checked using the element tools (Identify→Composite→Layer list) as illustrated in Fig. 6.

4.6 Impactor modeling

The assumption of an elastic body with no plastic deformation is appropriate for the low

velocity impact between the CFRP plate and the impactor made from a high-strength steel alloy, resulting in insignificant deformation of the impactor relative to the CFRP plate. Therefore, the impactor was modeled as a spherical rigid body of 25.4 mm diameter using the Shape_Mesher and the Sphere_Solid Entity. The rigid material model MAT_RIGID (MAT20) was used to define the steel material properties. The 8-node solid element size was 2 mm (average meshing size) to balance the simulation's accuracy and efficiency. The solid element formulation was defined using the default option of constant stress solid element (ELFORM 1), which has 3 degrees of freedom at each node.

The impactor's steel material has a modulus of elasticity as $E = 200$ GPa and Poisson's ratio as $\nu_{12} = 0.3$. If the rigid body interacts in a contact definition, these constants are used to determine sliding interface parameters. The realistic values for these constants should be defined. The inertial properties are calculated from the geometry and density of the rigid impactor specified in MAT20.

One way to satisfy the actual impact energy level of the spherical impactor with constant volume and initial velocity in the numerical simulation model is to replace the actual density of the impactor assembly to unrealistic value in MAT20. Therefore, theoretical a calculation was performed to determine the unrealistic density, which is outlined in the following steps:

The kinetic energy (KE) of the impact can be calculated using the impactor's mass (m) and initial velocity (v_i)

$$KE = \frac{1}{2} m v_i^2, \tag{9}$$

The density (ρ) is a function of the mass (m) and volume (V)

$$\rho = \frac{m}{V}, \tag{10}$$

The sphere volume (V) is defined using the diameter (d) of the impactor

$$V = \frac{1}{6} \pi d^3, \tag{11}$$

The density (ρ) can be obtained using Eqs. (9)-(11)

$$\rho = \frac{12(KE)}{\pi d^3 v_i^2}, \tag{12}$$

The unrealistic density is determined using Eq. (12), which is a function of 40 J kinetic energy (KE), 6.5 m/s initial velocity (v_i), and 0.0254 m diameter (d). After a slight calibration, the final unrealistic density was set to 223,600 kg/m^3. To confirm that the inputs in MAT20 are correct, the kinetic energy of the impactor was plotted in LS-Dyna with considering the impactor velocity.

4.7 Boundary conditions

The velocity of the spherical impactor is 6.5 m/s. Therefore, all impactor nodes have an initial translational velocity defined in negative global z-direction to achieve the specified level of impact energy (40 J) considering the mass of the impactor. INITIAL_VELOCITY_GENERATION card is used to define the transitional initial velocity of the impactor as the followings:

• VZ $= -6.5$ m/s.

The clamping conditions of the laminate include fixed support of the longitudinal edges and simple support of the lateral edges. Therefore, all nodes under the GFRP tabs (50 mm from both longitudinal ends) are set to fixed support, and the remaining nodes on the lateral sides are set to simple support. BOUNDARY_SPC_SET card is used to define the transitional and rotational boundary conditions.

4.8 Contact definition

In impact analysis, the deformations might be very substantial, making it difficult or impossible to predict where and how contact would occur. Since automated contacts are non-oriented and can detect penetration coming from either side of a shell element, the automatic contact options are recommended. Therefore, the contact type AUTOMATIC_ SURFACE_TO_SURFACE is used to define the contact algorithm between the steel impactor and CFRP plate. The impactor is defined as slave segment part ID (SSID), while the CFRP plate is defined as master segment part ID (MSID).

The static coefficient of friction (FS) between the steel material of the impactor and the CFRP material of the composite plate is set to 0.5, according to a published reference (Shi *et al.* 2020), and the dynamic coefficient of friction (FD) is set to 0.1, according to another published reference (Deka *et al.* 2008). These values are obtained from published work which shows good agreement to the experimental results.

4.9 Simulation control and output files

The simulation control and output files are essential for LS-DYNA simulations. The control files define the simulation parameters and guide the analysis, while the output files store the results for analysis and visualization. Using these files, users can run complex simulations, analyze model behavior, and gain insight into the simulated event. The following are essential steps used to define the impact simulation in this model:

- CONTROL_TERMINATION card is used to set the termination time (ENDTIM) to 0.008 seconds. This time was long enough to capture the entire impact event up to the rebound of the impactor.
- The numerical time step size is ignored. Therefore, the LS-dyna solver automatically calculates the minimum time step size for all elements considering length and density.
- The time interval between outputs (DT) is set to 4.0e-5 seconds for all recorded history outputs. This small value of the time interval between outputs allowed 202 output data increments, which shows a good output result.
- DATABASE_BINARY_D3PLOT is activated in this model. D3plot files are binary data generated by LS-DYNA during finite element model analysis. The file format " BINARY_D3plot " stores simulation results and post-processing data such as nodal displacements, velocities, accelerations, element stresses, strains, and other simulation results.
- DATABASE_ASCII_options in LS-Dyna are used to write the output files of the absorbed energy and the contact forces as the following:
  - MATSUM (Material Energies) is an ASCII file that contains the kinetic and internal energies for both the slave and master parts.
  - RCFORC (Resultant Interface Forces) is an ASCII file that contains the resultant contact forces for both the slave and master sides of each contact interface.

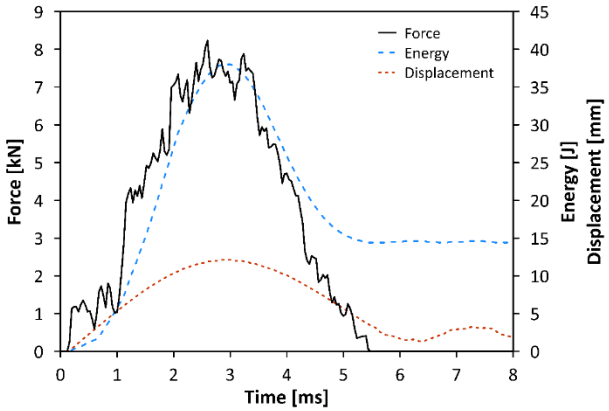

Fig. 7 Numerical simulation results of the impact force, energy and displacement

4.10 Numerical simulation results and validation

The numerical simulation results of the impact testing are plotted in terms of time-dependent plots of impact force, energy absorption, and deflection, as shown in Fig. 7. The numerical simulation results showed strong agreement with the experimental results in terms of energy, force, and displacement plots, as presented in Table 4. The absorbed energy value from the numerical simulation was very close to the experimental result, with a difference of 2.86%. Only 0.85% of the impact force value was different between the numerical simulation and the experimental result. The maximum deflection obtained from the numerical simulation was consistent with the experimental result, giving a value of 12.2 mm with no noticeable error.

In conclusion, the strong agreement shown between the numerical simulation results and the experimental results provides evidence of the efficacy of numerical simulation as a powerful predictive technique to evaluate the impact behavior of the unidirectional fiber-reinforced composites. The MAT54 material model and the PART_COMPOSITE feature in LS-Dyna can be valuable tools for defining composite materials with tuning parameters, particularly when the objective is to model multi-layer composite material in a single shell model. This will provide confidence to the results and findings when the curved plates and bio-inspired layup were applied.

5. Numerical simulation model

The numerical simulation model used to validate the experimental results is used again with different curved plate geometries (R0, R500, R750, and R1500) and different layup configurations (UD, CP, QI, LH, and FH) to improve the impact resistance of the composite structures. The low velocity impact conditions and the boundary condition of the CFRP plate are fixed without any change. Only the number of layers increased from 24 up to 32 layers (single layer thickness is 0.1125 mm), which results in a total laminate thickness of 3.6 mm. PART_COMPOSITE feature is used to define the fibers orientation of the different layup configurations. The MAT54 input parameters for material properties are similar to the used parameters in the validation model, which are presented in Table 3. The sample layout (for the R500 case) of the numerical simulation models is illustrated in Fig. 8. The front view of all model cases is presented in Fig. 9.

Table 3 The main input parameter for material MAT54

Variable	Description	Value	Comment
RO	Mass density, ρ	1620	ρ, from Table.1
EA	Young's modulus in longitudinal direction	153e+9	E_1, from Table.1
EB	Young's modulus in transverse direction	10.3e+9	E_2, from Table.1
PRBA	Poisson's ratio, ν_{21} (minor)	0.0202	$\nu_{21} = \nu_{12}\,(E_2/E_1)$
PRCA	Poisson's ratio, ν_{31} (minor)	0.0202	Similar to PRBA
GAB	Shear modulus, G_{12}	5.2e+9	G_{12}, From Table.1
GBC	Shear modulus, G_{23}	2.2e+9	E_1, E_2 and PRBA
GCA	Shear modulus, G_{31}	5.2e+9	Similar to GAB
TFAIL	Time step size for element deletion	1.e-07	From published work [53,55]
SOFT	Softening reduction factor for material strength in crashfront elements.	1.8	Calibrated value
XC	Longitudinal compressive strength, σ_{11}^{-}	1.5e+9	σ_{11}^{-}, from Table.1
XT	Longitudinal tensile strength, σ_{11}^{+}	2.54e+9	σ_{11}^{+}, from Table.1
YC	Transverse compressive strength, σ_{22}^{-}	236e+6	σ_{22}^{-}, from Table.1
YT	Transverse tensile strength, σ_{22}^{+}	82e+6	σ_{22}^{+}, from Table.1
SC	Shear strength, τ_{12}	90e+6	τ_{12}, from Table.1
CRIT	Failure criterion (material number)	54.0	Chang failure criterion
PFL	Percentage of layers must fail until crashfront is initiated	70	Estimated value
SLIMT1	Factor for minimum stress limit after stress maximum (fiber tension)	0.01	From MAT58 Document
SLIMC1	Factor for minimum stress limit after stress maximum (fiber compression)	1.0	From MAT58 Document
SLIMT2	Factor for minimum stress limit after stress maximum (matrix tension)	1.0	From MAT58 Document
SLIMC2	Factor for minimum stress limit after stress maximum (matrix compression)	1.0	From MAT58 Document
SLIMCS	Factor for minimum stress limit after stress maximum (shear)	1.0	From MAT58 Document
NCYRED	Number of cycles for stress reduction from maximum to minimum	5.0	From MAT58 Document
SOFTG	Softening reduction factor for transverse shear moduli GBC and GCA	1.0	Default

Table 4 Comparison between the experimental results and numerical simulation results

Material	Experimental results [49]	Numerical simulation	Error (%)
Absorbed Energy (J)	14.00	14.40	2.86%
Impact Force (kN)	8.30	8.23	0.85%
Max. Deflection (mm)	12.20	12.20	0.00%

6. Results and discussions

The final simulation results of the different plate curvatures (R0 (Flate), R500, R750, and R1500) and layup configurations (UD, CP, QI, LH, and FH) are presented in Table 5. These results include the impact force in (kN), absorbed energy (J), and maximum deflection (mm).

Table 5 The results of the different plate curvatures and layup configurations

Designation-Layup Configuration	Impact Force [kN]	Absorbed Energy [J]	Max. Deflection [mm]
UD (FLAT)	10.8	11.7	11.0
UD (R1500)	6.8	15.6	14.6
UD (R750)	9.0	17.4	9.4
UD (R500)	6.3	16.5	10.9
CP (FLAT)	8.7	20.1	10.4
CP (R1500)	8.2	21.2	11.4
CP (R750)	7.1	20.1	10.2
CP (R500)	7.1	19.1	9.3
QI (FLAT)	9.6	15.3	9.6
QI (R1500)	8.5	17.0	10.3
QI (R750)	9.0	17.5	9.4
QI (R500)	8.0	17.3	9.1
LH (FLAT)	9.0	17.8	9.6
LH (R1500)	9.6	17.1	10.4
LH (R750)	9.1	16.9	9.6
LH (R500)	7.7	16.8	9.2
FH (FLAT)	10.1	22.3	10.2
FH (R1500)	7.4	12.3	11.9
FH (R750)	7.7	12.9	10.2
FH (R500)	7.9	15.2	9.7

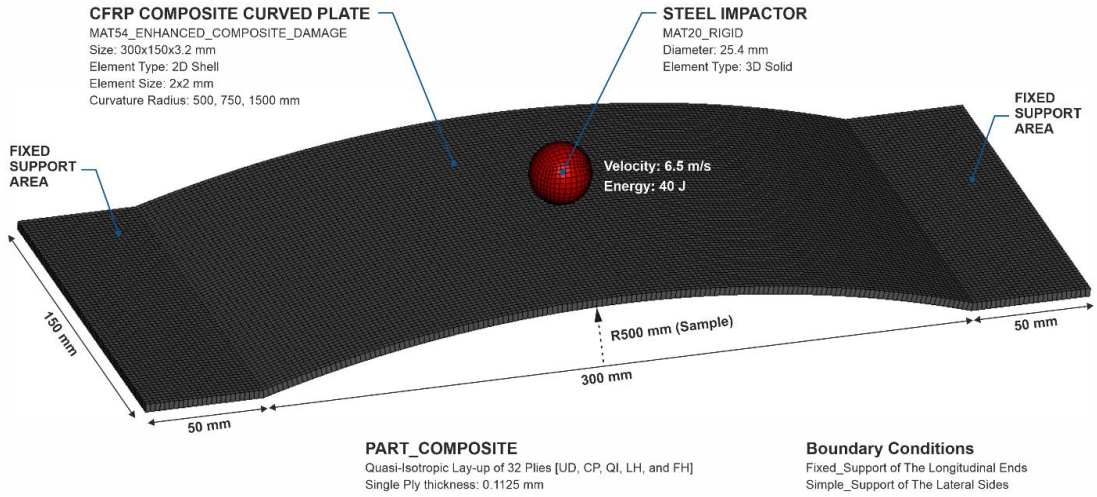

Fig. 8 Sample layout (for R500 Case) of the numerical simulation model

Fig. 10 shows that the different plate curvatures and layup configurations can affect the final impact behavior in terms of impact force, energy absorption, and deflection. For all cases, the below findings present the higher and lower values:

• The UD (FLAT) plate showed the highest impact force at 10.8 kN, while the UD (R500) plate showed the lowest impact force at 6.3 kN.

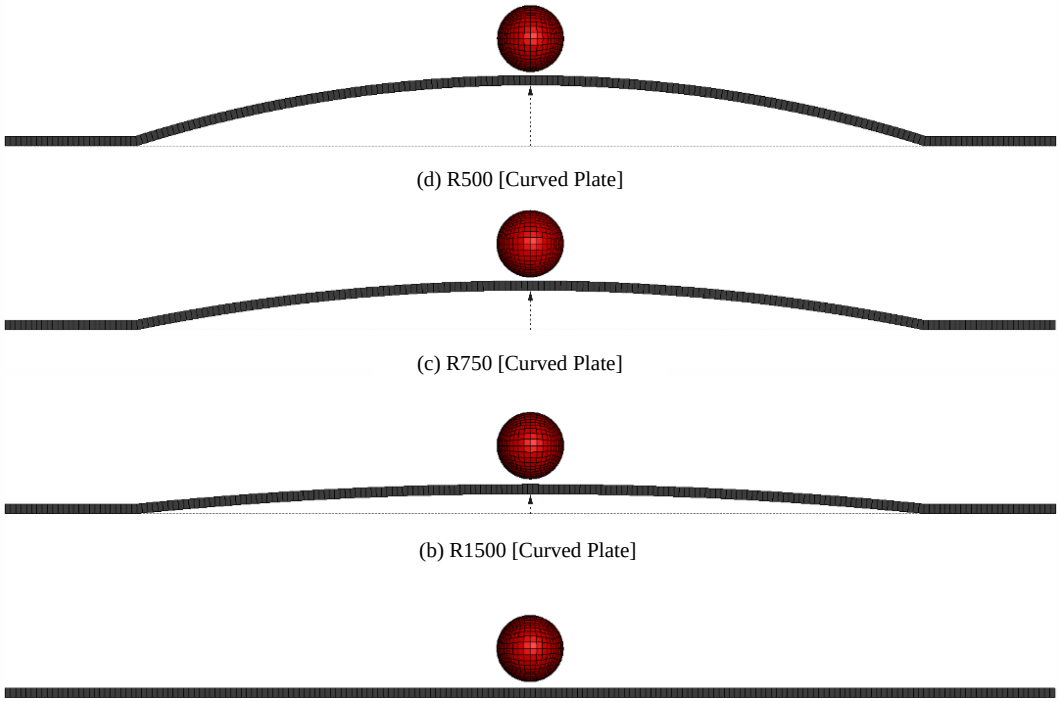

(d) R500 [Curved Plate]

(c) R750 [Curved Plate]

(b) R1500 [Curved Plate]

(a) R0 [Flat Plate]

Fig. 9 Front view of impacted flat and curved plates

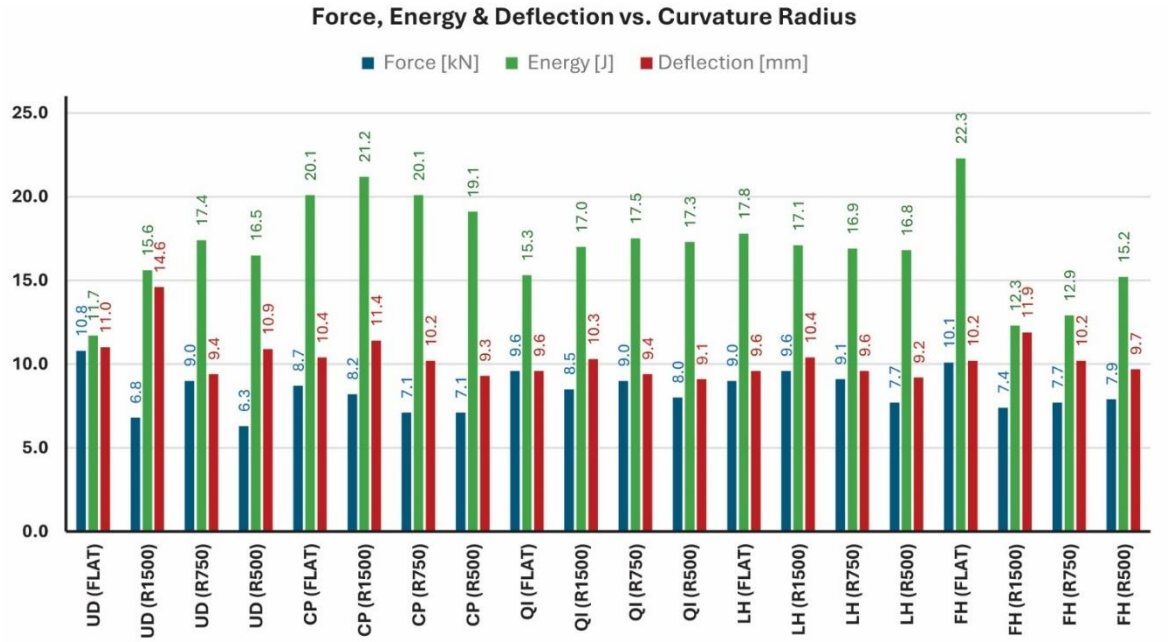

Fig. 10 Force, energy & deflection vs. curvature radius

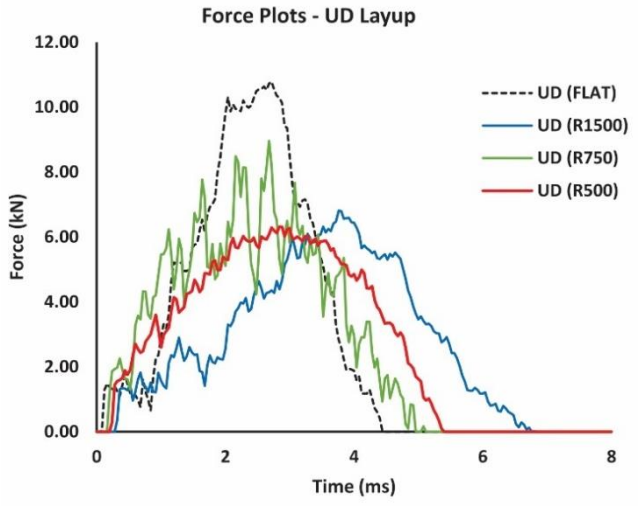

Fig. 11 Force plots-UD layup

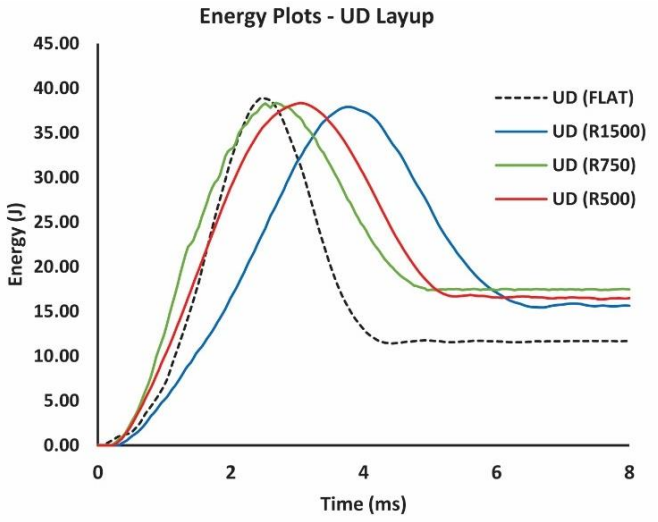

Fig. 12 Energy plots-UD layup

• The FH (FLAT) plate showed the highest impact energy at 22.3 J, while the UD (FLAT) plate showed the lowest impact energy at 11.7 J.

• The UD (R1500) plate showed the highest deflection at 14.6 mm, while the QI (R500) plate showed the lowest deflection at 9.1 mm.

Each layup configuration (UD, CP, QI, LH, and FH) will be analyzed separately with different plate curvatures (Flat, R1500, R750, and R500). The main purpose is to discover the advantages of the curved plates over the flat plate in order to improve the low velocity impact resistance. By comparing the results, it will be useful to identify the optimal layup configuration and curvature that maximize impact resistance while maintaining efficiency. The findings and discussions are listed in the following topics.

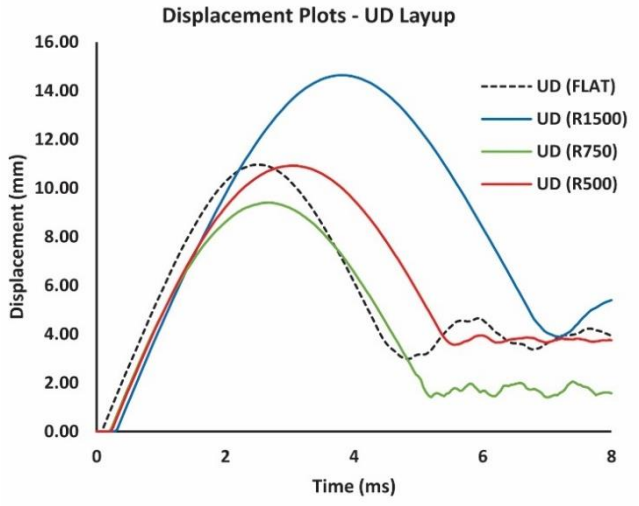

Fig. 13 Displacement plots-UD layup

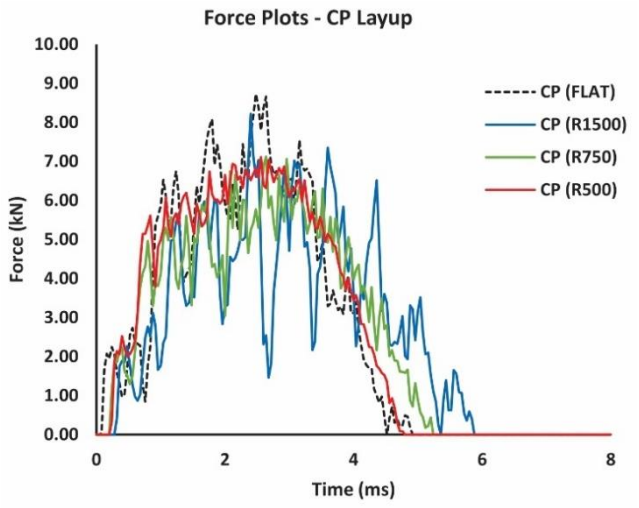

Fig. 14 Force plots-CP layup

6.1 UD layup results

For the UD layup configuration (Figs. 11-13):

• The UD (FLAT) plate showed the higher impact force value (10.8 kN) compared with other curved plates, which indicates that the curved plates can reduce the impact force level. A higher oscillation rate is noticed for the impact force diagram of the UD (R750).

• The UD (FLAT) plate showed the lower absorbed energy value (11.7 J) compared with other curved plates (15.6-17.4 J), which illustrates the energy absorption capability of the curved plates.

• The UD (R750) plate showed the lower deflection value (9.4 mm), while the UD (R1500) plate showed the higher deflection value (14.6 mm). Thus, the UD curved plate can either

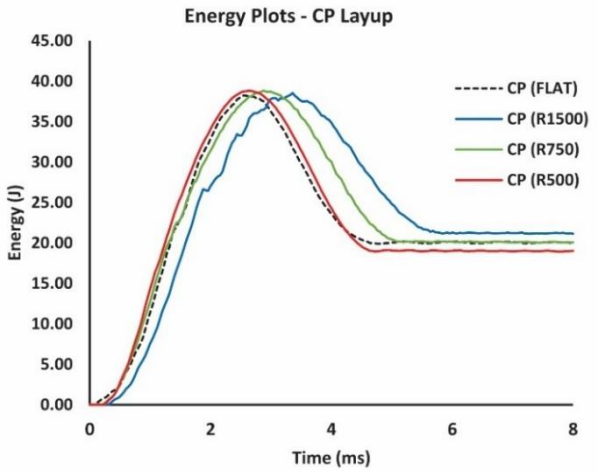

Fig. 15 Energy plots-CP layup

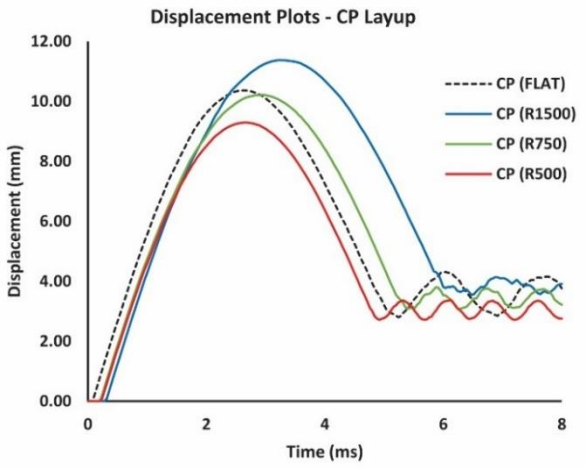

Fig. 16 Displacement plots-CP layup

reduce or increase the deflection level compared with the UD (FLAT) plate (11.0 mm).

6.2 CP layup results

For the CP layup configuration (Figs. 14-16):

• The CP (FLAT) plate showed a slightly higher impact force value (8.7 kN) compared with other curved plates. The CP (R500) showed the lower oscillation rate in the impact force diagram.

• The CP (FLAT) plate and all curved plates showed closer energy absorption levels (19.1-21.2 J), where there is no clear advantage shown for the curved plates.

• The CP (R500) plate showed the lower deflection value (9.3 mm), while the CP (R1500) plate showed the higher deflection value (11.4 mm). Thus, the CP curved plate can either reduce or increase the deflection level compared with the CP (FLAT) plate value (10.4 mm).

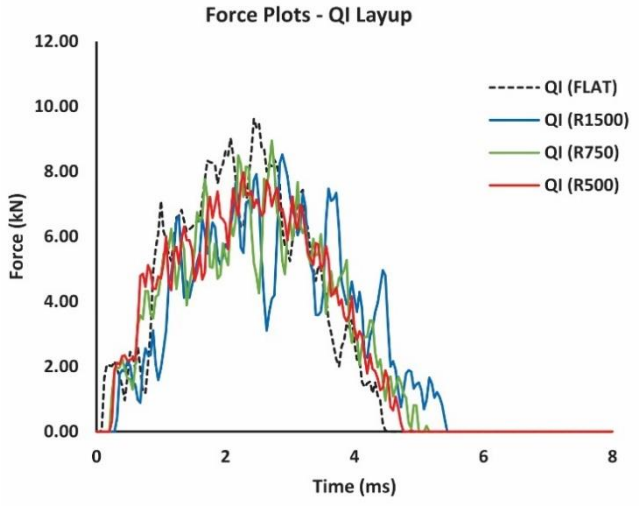

Fig. 17 Force plots-QI layup

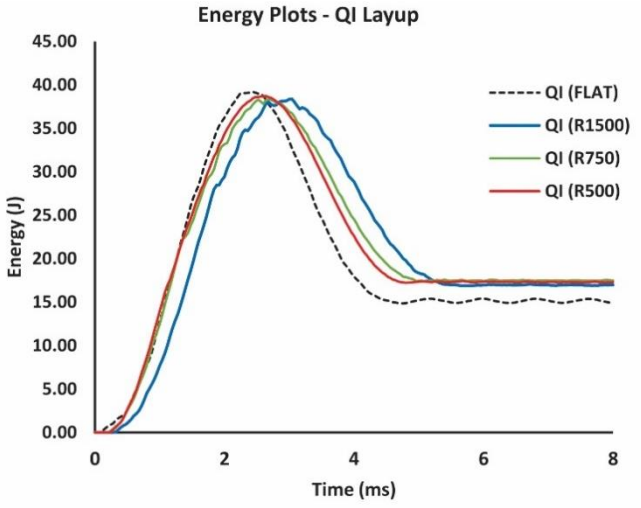

Fig. 18 Energy plots-QI layup

6.3 QI layup results

For the QI layup configuration (Figs. 17-19):

• The QI (R500) plate showed the lower impact force (8.0 kN) and lower oscillation rate, compared with all other plates. Where the QI (FLAT) plate showed the higher impact force (9.6 kN), which indicates that the curved plates can reduce the impact force level.

• The QI (FLAT) plate showed the lower absorbed energy value (15.3 J), compared with other curved plates (17.0-17.5 J), that illustrate the energy absorption capability of the curved plates.

• The QI (R500) plate showed the lower deflection value (9.1 mm), while the QI (R1500) plate showed the higher deflection value (10.3 mm). Thus, the QI curved plate can either reduce or increase the deflection level compared with the QI (FLAT) plate value (9.6 mm).

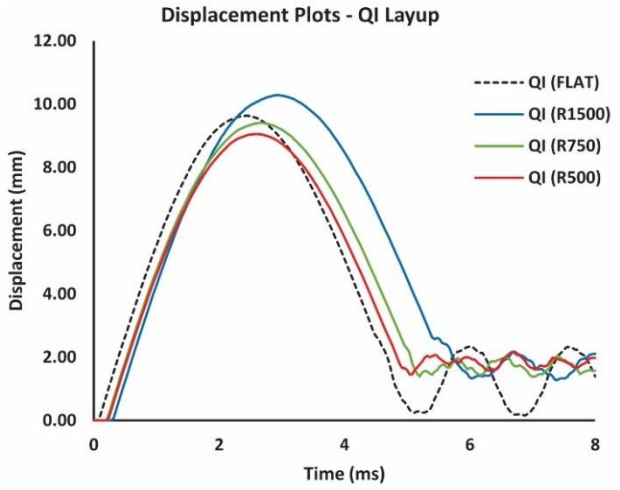

Fig. 19 Displacement Plots - QI Layup

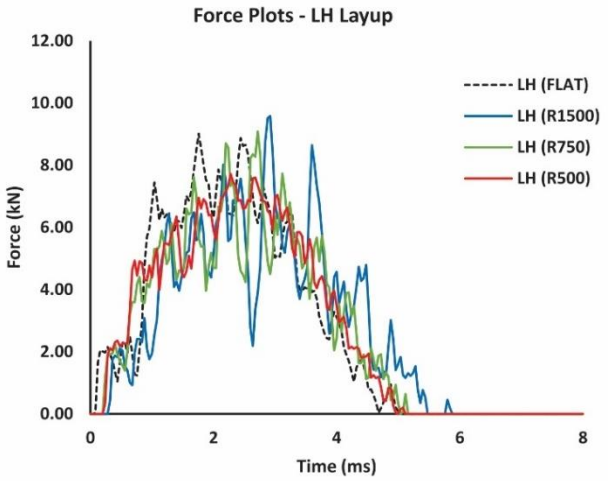

Fig. 20 Force plots-LH layup

6.4 LH layup results

For the LH layup configuration (Figs. 20-22):

• The LH (R500) plate showed the lower impact force (7.7 kN) and lower oscillation rate, compared with all other plates. Where the LH (R1500) plate showed the higher impact force (9.6 kN), which indicates that the curved plates can reduce the impact force level.

• The LH (FLAT) plate showed the higher absorbed energy value (17.8 J), compared with other curved plates that showed closer values (16.8-17.1 J), where there is no clear advantage shown for the curved plates energy absorption.

• The LH (R500) plate showed the lower deflection value (9.2 mm), while the LH (R1500) plate showed the higher deflection value (10.4 mm). Thus, the LH curved plate can either reduce or increase the deflection level compared with the LH (FLAT) plate value (9.6 mm).

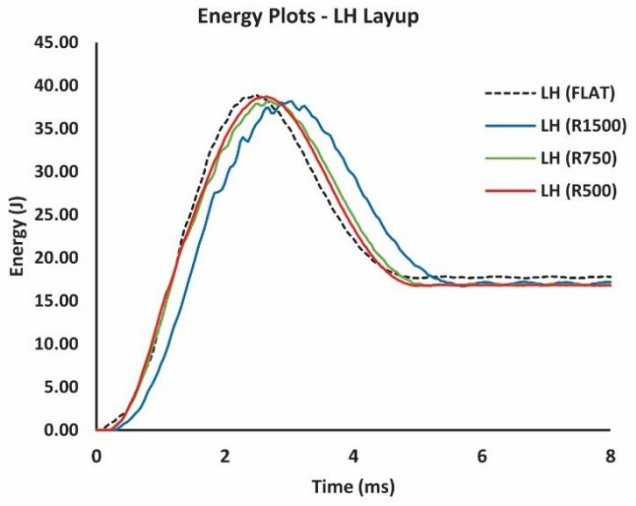

Fig. 21 Energy plots-LH layup

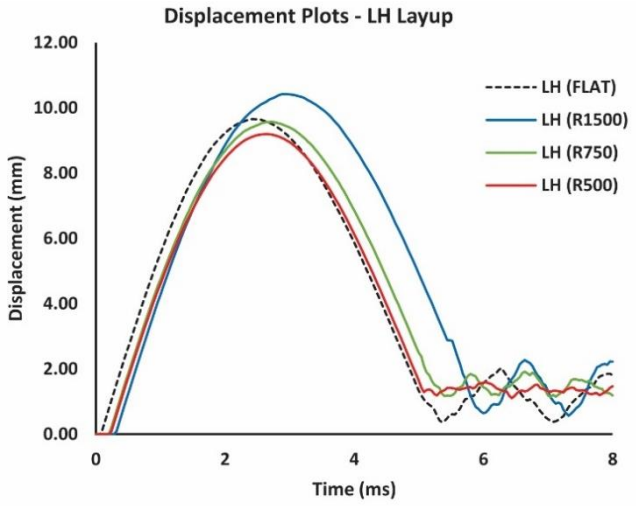

Fig. 22 Displacement plots-LH layup

6.5 FH layup results

For the FH layup configuration (Fig. 23-25):

• The FH (FLAT) plate showed the higher impact force (10.1 kN), compared with all curved plates (7.4-7.9 kN), which indicates that the curved plates can reduce the impact force level. All the FH plates showed low oscillation rates for the impact force diagrams.

• The FH (FLAT) plate showed the higher absorption energy value (22.3 J) compared with all other curved plates (12.3-15.2 J).

The FH (R500) plate showed the lower deflection value (9.7 mm), while the FH (R1500) plate showed the higher deflection value (11.2 mm). Thus, the FH curved plate can either reduce or increase the deflection level compared with the FH (FLAT) plate value (10.2 mm).

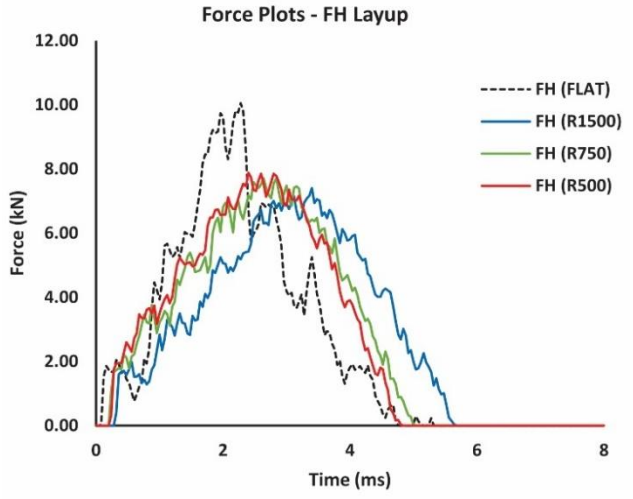

Fig. 23 Force plots-FH layup

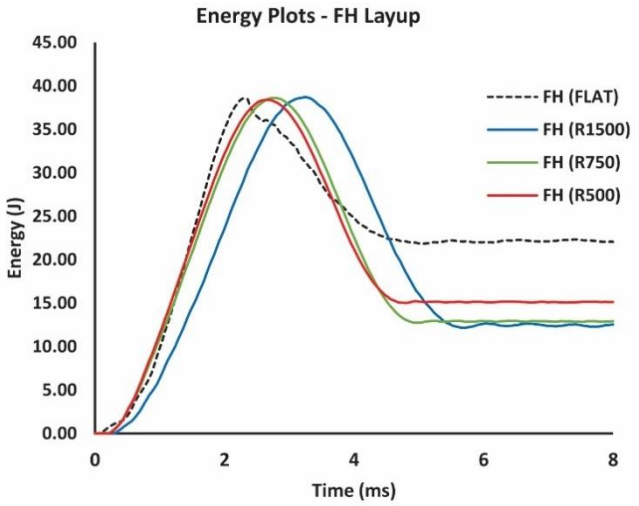

Fig. 24 Energy plots-FH layup

In conclusion, the curved plates showed excellent behavior in reducing the impact force and deflection during the low velocity impact simulation for all layup configurations. Table 6 and Table 7 present the maximum reduction in impact force and deflection of the curved plates compared to flat plates. Comparing with the FLAT plate, the R500 plate (which has the higher curvature rate) showed an outstanding performance in reducing the impact force for the UD, CP, QI, and LH layup configurations and reducing the maximum deflection for the CP, QI, LH, and FH layup configurations. This indicates that the curved plates can be a useful technique in controlling the impact response, where the selection of the layup configurations for the curved plates can be effective in enhancing structural impact resistance under low velocity impact conditions. Future studies could explore the long-term durability and performance of the curved plates under various impact conditions.

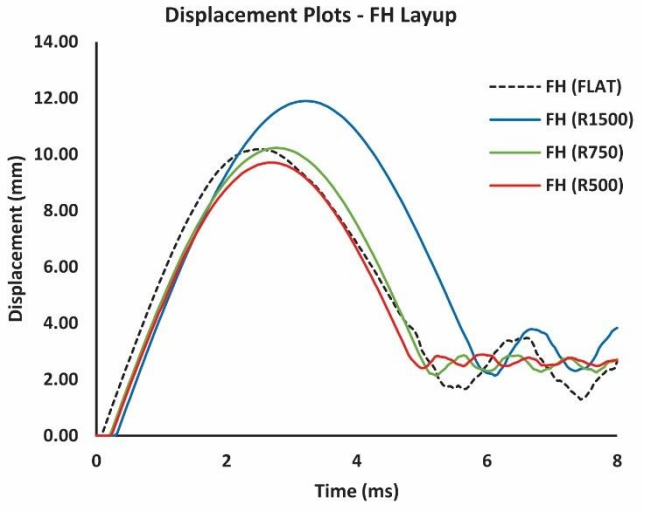

Fig. 25 Displacement plots-FH layup

Table 6 The maximum reduction in impact force of the curved plates compared with flat plates

Layup	Plate Designation	Impact Force [kN]	Reduction [%]
UD	FLAT	10.8	-41.7%
	R500	6.3	
CP	FLAT	8.7	-18.4%
	R500	7.1	
QI	FLAT	9.6	-16.7%
	R500	8.0	
LH	FLAT	9.0	-14.4%
	R500	7.7	
FH	FLAT	10.1	-26.7%
	R1500	7.4	

Table 7 The maximum reduction in deflection of the curved plates compared with flat plates

Layup	Plate Designation	Deflection [mm]	Reduction [%]
UD	FLAT	11.0	-14.5%
	R750	9.4	
CP	FLAT	10.4	-10.6%
	R500	9.3	
QI	FLAT	9.6	-5.2%
	R500	9.1	
LH	FLAT	9.6	-4.2%
	R500	9.2	
FH	FLAT	10.2	-4.9%
	R500	9.7	

7. Conclusions

A numerical simulation model is as developed using the commercial explicit finite element code LS-DYNA to investigate the load response of the low velocity impact for curved plates with different layup configurations using unidirectional carbon fiber-reinforced polymer (CFRP).

At first, the numerical simulation model was developed to validate the findings of a published experimental work for the low velocity impact of a CFRP plate. The numerical simulation results showed strong agreement with the experimental results in terms of absorbed energy, impact force, and deflection plots. The main findings include:

- The absorbed energy value from the numerical simulation (14.40 J) was very close to the experimental result (14.00 J), with a difference of 2.86%.
- The impact force value from the numerical simulation (8.23 kN) was lower than the experimental result (8.30 kN) with a difference of only 0.85%.
- The maximum deflection obtained from the numerical simulation (12.20 mm) was consistent with the experimental result (12.20 mm) with no noticeable error.

Consequently, based on the validated numerical simulation model, different curved plates and layup configurations have been considered to investigate the impact load response of the composite structures. The curved radii in mm include the following: R0 (Flate), R500, R750, and R1500. The layup configurations include the following: Unidirectional (UD), Cross-Ply (CP), Quasi-Isotropic (QI), linear bio-inspired, known as Linear-Helicoidal 24° (LH), and non-linear bio-inspired, known as Fibonacci-Helicoidal (FH). The designed CFRP plate consist of 32-plies with overall dimensions of 300x150x3.6 mm. The CFRP plate is impacted by a hemispherical steel impactor of 25.4 mm diameter and 6.5 m/s speed to generate 40 J of impact energy. Each layup configuration was analyzed separately with different plate curvatures to discover the advantages of the curved plates over the flat plate to improve the low velocity impact resistance. The main findings are listed as follows:

- The curved plates showed excellent behavior in reducing the impact force and deflection during the low velocity impact simulation for all layup configurations.
- The R500 plate (which has the higher curvature rate) showed an outstanding performance in reducing the impact force for the UD, CP, QI, and LH layup configurations and reducing the maximum deflection for the CP, QI, LH, and FH layup configurations.

It can be concluded from this study that the MAT54 material model and the PART_COMPOSITE feature in LS-Dyna can be valuable tools for representing composite materials with tuning parameters, particularly when the objective is to model a multi-layer composite material in a single shell model. The curved plates can be a useful technique in controlling the impact response, where the selection of the layup configurations for the curved plates can be effective in enhancing structural impact resistance under low velocity impact conditions. The developed numerical simulation model can be effectively utilized for the purpose of designing and analyzing innovative bio-inspired composite structures in various configurations under different impact scenarios to study the load response.

References

Ahmed, M.M., Dhakal, H.N., Zhang, Z.Y., Barouni, A. and Zahari, R. (2021), “Enhancement of impact toughness and damage behaviour of natural fibre reinforced composites and their hybrids through novel

improvement techniques: A critical review", *Compos. Struct.*, **259**, 113496. https://doi.org/10.1016/j.compstruct.2020.113496.

Alessi,, Y.A., Ali, I.A, Alazwari, M.A., Almitani, K.H., Abdelrahman, A. and Eltaher, M.A. (2023), "Dynamic analysis of piezoelectric perforated cantilever bimorph energy harvester via finite element analysis", *Adv. Aircraft Spacecraft Sci.*, **10**(2), 179-202. https://doi.org/10.12989/aas.2023.10.2.179.

Amaro, A.M., Santos, J.B. and Cirne, J.S. (2011), "Delamination depth in composites laminates with interface elements and ultrasound analysis", *Strain*, **47**(2), 138-145. https://doi.org/10.1111/j.1475-1305.2008.00491.x.

Aoki, Y., Suemasu, H. and Ishikawa, T. (2007), "Damage propagation in CFRP laminates subjected to low velocity impact and static indentation", *Adv. Compos. Mater.*, **16**(1), 45-61.https://doi.org/10.1163/156855107779755318.

Atas, C., Akgun, Y., Dagdelen, O., Icten, B.M. and Sarikanat, M. (2011), "An experimental investigation on the low velocity impact response of composite plates repaired by VARIM and hand lay-up processes", *Compos. Struct.*, **93**(3), 1178-1186. https://doi.org/10.1016/j.compstruct.2010.10.002.

Aymerich, F., Dore, F. and Priolo, P. (2008), "Prediction of impact-induced delamination in cross-ply composite laminates using cohesive interface elements", *Compos. Sci. Technol.*, **68**(12), 2383-2390. https://doi.org/10.1016/j.compscitech.2007.06.015.

Aymerich, F., Dore, F. and Priolo, P. (2009), "Simulation of multiple delaminations in impacted cross-ply laminates using a finite element model based on cohesive interface elements", *Compos. Sci. Technol.*, **69**(11-12), 1699-1709. https://doi.org/10.1016/j.compscitech.2008.10.025.

Baakeel, F., Eltaher, M.A., Basha, M.A. and Abdelwahed, M.A. (2025), "Impact response of bio-inspired laminated composite plates:A numerical simulation model using 2D shell element", *Steel Compos. Struct.*, **54**(1), 33-52. https://doi.org/10.12989/scs.2025.54.1.033.

Baakeel, F., Eltaher, M.A., Basha, M.A., Melibari, A. and Abdelrhman, A.A. (2023), "Static and modal analysis of bio-inspired laminated composite shells using numerical simulation", *Adv. Aircraft Spacecraft Sci.*, **10**(4), 347-368. https://doi.org/10.12989/aas.2023.10.4.347.

Bhaskar, D.P. and Thakur, A.G. (2019), "FE modeling for geometrically nonlinear analysis of laminated plates using a new plate theory", *Adv. Aircraft Spacecraft Sci.*, **6**(5), 409-426. https://doi.org/10.12989/aas.2019.6.5.409.

Bouvet, C., Castanié, B., Bizeul, M. and Barrau, J.J. (2009), "Low velocity impact modelling in laminate composite panels with discrete interface elements", *Int. J. Solid. Struct.*, **46**(14-15), 2809-2821. https://doi.org/10.1016/j.ijsolstr.2009.03.010.

Bouvet, C., Hongkarnjanakul, N., Rivallant, S. and Barrau, J.J. (2013), "Discrete impact modeling of inter- and intra-laminar failure in composites", *Dynamic Failure of Composite and Sandwich Structures*, 339-392. https://doi.org/10.1007/978-94-007-5329-7_8.

Camanho, P.P., Davila, C.G. and De Moura, M.F. (2003), "Numerical simulation of mixed-mode progressive delamination in composite materials", *J. Compos. Mater.*, **37**(16), 1415-1438. https://doi.org/10.1177/0021998303034505.

Caprino, G., Carrino, L., Durante, M., Langella, A. and Lopresto, V. (2015), "Low impact behaviour of hemp fibre reinforced epoxy composites", *Compos. Struct.*, **133**, 892-901. https://doi.org/10.1016/j.compstruct.2015.08.029.

Chang, F.K. and Chang, K.Y. (1987), "A progressive damage model for laminated composites containing stress concentrations", *J. Compos. Mater.*, **21**(9), 834-855. https://doi.org/10.1177/002199838702100904.

Cherniaev, A., Butcher, C. and Montesano, J. (2018), "Predicting the axial crush response of CFRP tubes using three damage-based constitutive models", *Thin Wall. Struct.*, **129**, 349-364. https://doi.org/10.1016/j.tws.2018.05.003.

De Moura, M.F.S.F. and Gonçalves, J.P.M. (2004), "Modelling the interaction between matrix cracking and delamination in carbon-epoxy laminates under low velocity impact", *Compos. Sci. Technol.*, **64**(7-8), 1021-1027. https://doi.org/10.1016/j.compscitech.2003.08.008.

De Vasconcellos, D.S., Sarasini, F., Touchard, F., Chocinski-Arnault, L., Pucci, M., Santulli, C., ... & Sorrentino, L. (2014), "Influence of low velocity impact on fatigue behaviour of woven hemp fibre

reinforced epoxy composites", *Compos. Part B: Eng.*, **66**, 46-57. https://doi.org/10.1016/j.compositesb.2014.04.025.
Deka, L.J., Bartus, S.D. and Vaidya, U.K. (2008), "Damage evolution and energy absorption of E-glass/polypropylene laminates subjected to ballistic impact", *J. Mater. Sci.*, **43**, 4399-4410. https://doi.org/10.1007/s10853-008-2595-0.
Donadon, M.V., Iannucci, L., Falzon, B.G., Hodgkinson, J.M. and de Almeida, S.F. (2008), "A progressive failure model for composite laminates subjected to low velocity impact damage", *Comput. Struct.*, **86**(11-12), 1232-1252. https://doi.org/10.1016/j.compstruc.2007.11.004.
Faggiani, A. and Falzon, B.G. (2010), "Predicting low-velocity impact damage on a stiffened composite panel", *Compos. Part A: Appl. Sci. Manuf.*, **41**(6), 737-749. https://doi.org/10.1016/j.compositesa.2010.02.005.
Feraboli, P., Wade, B., Deleo, F., Rassaian, M., Higgins, M. and Byar, A. (2011), "LS-DYNA MAT54 modeling of the axial crushing of a composite tape sinusoidal specimen", *Compos. Part A: Appl. Sci. Manuf.*, **42**(11), 1809-1825. https://doi.org/10.1016/j.compositesa.2011.08.004.
Fuga, F.R. and Donadon, M.V. (2021), "Low velocity impact on pre-loaded composite plates: a novel standard-based experimental apparatus", *Compos. Struct.*, **261**, 113315. https://doi.org/10.1016/j.compstruct.2020.113315.
Gebhardt, J., Schlamp, M., Ehrlich, I. and Hiermaier, S. (2023), "Low-velocity impact behavior of elliptic curved composite structures", *Int. J. Impact Eng.*, **180**, 104663. https://doi.org/10.1016/j.ijimpeng.2023.104663.
Guo-dong, F., Jun, L. and Bao-lai, W. (2009), "Progressive damage and nonlinear analysis of 3D four-directional braided composites under unidirectional tension", *Compos. Struct.*, **89**(1), 126-133. https://doi.org/10.1016/j.compstruct.2008.07.016.
Hahn, H.T. and Tsai, S.W. (1973), "Nonlinear elastic behavior of unidirectional composite laminae", *J. Compos. Mater.*, **7**(1), 102-118. https://doi.org/10.1177/002199837300700108.
Hashin, Z. (1980), "Failure criteria for unidirectional fiber composites", *J. Appl. Mech.*, **47**(2), 329-334.
Hashin, Z. and Rotem, A. (1973), "A fatigue failure criterion for fiber reinforced materials", *J. Compos. Mater.*, **7**(4), 448-464. https://doi.org/10.1177/002199837300700404.
Heimbs, S., Heller, S., Middendorf, P., Hähnel, F. and Weiße, J. (2009), "Low velocity impact on CFRP plates with compressive preload: Test and modelling", *Int. J. Impact Eng.*, **36**(10-11), 1182-1193. https://doi.org/10.1016/j.ijimpeng.2009.04.006.
Hou, J.P., Petrinic, N. and Ruiz, C. (2001), "A delamination criterion for laminated composites under low-velocity impact", *Compos. Sci. Technol.*, **61**(14), 2069-2074. https://doi.org/10.1016/S0266-3538(01)00128-2.
Hou, J.P., Petrinic, N., Ruiz, C. and Hallett, S.R. (2000), "Prediction of impact damage in composite plates", *Compos. Sci. Technol.*, **60**(2), 273-281. https://doi.org/10.1016/S0266-3538(99)00126-8.
Iannucci, L. and Ankersen, J. (2006), "An energy based damage model for thin laminated composites", *Compos. Sci. Technol.*, **66**(7-8), 934-951. https://doi.org/10.1016/j.compscitech.2005.07.033.
Jayatilake, I.N., Karunasena, W. and Lokuge, W. (2016), "Finite element based dynamic analysis of multilayer fibre composite sandwich plates with interlayer delaminations", *Adv. Aircraft Spacecraft Sci.*, **3**(1), 015. https://doi.org/10.12989/aas.2016.3.1.015.
Jordan, J.B., Naito, C.J. and Haque, B.Z. (2014), "Quasi-static, low-velocity impact and ballistic impact behavior of plain weave E-glass/phenolic composites", *J. Compos. Mater.*, **48**(20), 2505-2516. https://doi.org/10.1177/0021998313499952.
Kaci, D.A., Madani, K., Mokhtari, M., Feaugas, X. and Touzain, S. (2017), "Impact of composite patch on the J-integral in adhesive layer for repaired aluminum plate", *Adv. Aircraft Spacecraft Sci.*, **4**(6), 679. https://doi.org/10.12989/aas.2017.4.6.679.
Karamanli, A., Vo, T.P. and Eltaher, M.A. (2024), "Comprehensive analysis of bio-inspired laminated composites plates using a quasi-3D theory and higher order FE models", *Thin Wall. Struct.*, **198**, 111735. https://doi.org/10.1016/j.tws.2024.111735.
Kim, S.J., Goo, N.S. and Kim, T.W. (1997), "The effect of curvature on the dynamic response and impact-

induced damage in composite laminates", *Compos. Sci. Technol.*, **57**(7), 763-773. https://doi.org/10.1016/S0266-3538(97)80015-2.

Kravchenko, S.G., Volle, C. and Kravchenko, O.G. (2021), "An experimental investigation on low-velocity impact response and compression after impact of a stochastic, discontinuous prepreg tape composite", *Compos. Part A: Appl. Sci. Manuf.*, **149**, 106524. https://doi.org/10.1016/j.compositesa.2021.106524.

Krishnamurthy, K.S., Mahajan, P. and Mittal, R.K. (2003), "Impact response and damage in laminated composite cylindrical shells", *Compos. Struct.*, **59**(1), 15-36. https://doi.org/10.1016/S0263-8223(02)00238-6.

Kurşun, A., Şenel, M. and Enginsoy, H.M. (2015), "Experimental and numerical analysis of low velocity impact on a preloaded composite plate", *Adv. Eng. Softw.*, **90**, 41-52. https://doi.org/10.1016/j.advengsoft.2015.06.010.

Lapczyk, I. and Hurtado, J.A. (2007), "Progressive damage modeling in fiber-reinforced materials", *Compos. Part A: Appl. Sci. Manuf.*, **38**(11), 2333-2341. https://doi.org/10.1016/j.compositesa.2007.01.017.

Lee, C.S., Kim, J.H., Kim, S.K., Ryu, D.M. and Lee, J.M. (2015), "Initial and progressive failure analyses for composite laminates using Puck failure criterion and damage-coupled finite element method", *Compos. Struct.*, **121**, 406-419. https://doi.org/10.1016/j.compstruct.2014.11.011.

Liang, S., Guillaumat, L. and Gning, P.B. (2015), "Impact behaviour of flax/epoxy composite plates", *Int. J. Impact Eng.*, **80**, 56-64. https://doi.org/10.1016/j.ijimpeng.2015.01.006.

Liu, P.F., Liao, B.B., Jia, L.Y. and Peng, X.Q. (2016), "Finite element analysis of dynamic progressive failure of carbon fiber composite laminates under low velocity impact", *Compos. Struct.*, **149**, 408-422. https://doi.org/10.1016/j.compstruct.2016.04.012.

LS-DYNA Keyword User's Manual (2007), Version 971, Livermore, CA, Livermore Software Technology Corporation.

Maamar, D.B. and Ramdane, Z. (2016), "Characterization of the mechanical behaviour of carbon fiber composite laminate under low velocity impact", *Periodica Polytechnica Mech. Eng.*, **60**(3), 142-151. https://doi.org/10.3311/PPme.8633.

Metoui, S., Pruliere, E., Ammar, A. and Dau, F. (2018), "A reduced model to simulate the damage in composite laminates under low velocity impact", *Compos. Struct.*, **199**, 34-45. https://doi.org/10.1016/j.compstruc.2018.01.012.

Miao, H., Wu, Z., Ying, Z. and Hu, X. (2019), "The numerical and experimental investigation on low-velocity impact response of composite panels: Effect of fabric architecture", *Compos. Struct.*, **227**, 111343. https://doi.org/10.1016/j.compstruct.2019.111343.

Mohamed, N., Mohamed, S.A., Abdelrhmaan, A.A. and Eltaher, M.A. (2023), "Nonlinear stability of bio-inspired composite beams with higher order shear theory", *Steel Compos. Struct.*, **46**(6), 759-772. https://doi.org/10.12989/scs.2023.46.6.759.

Mohamed, S.A., Mohamed, N. and Eltaher, M.A. (2022), "Bending, buckling and linear vibration of bio-inspired composite plates", *Ocean Eng.*, **259**, 111851. https://doi.org/10.1016/j.oceaneng.2022.111851

Rachid, Z., Kaddour, R. and Achache, H. (2018), "Dynamic calculation of a tapered shaft rotor made of composite material", *Adv. Aircraft Spacecraft Sci.*, **5**(1), 051. https://doi.org/10.12989/aas.2018.5.1.051.

Saghafi, H., Minak, G. and Zucchelli, A. (2014), "Effect of preload on the impact response of curved composite panels", *Compos. Part B: Eng.*, **60**, 74-81. https://doi.org/10.1016/j.compositesb.2013.12.026.

Sanchez, C., Arribart, H. and Giraud Guille, M.M. (2005), "Biomimetism and bioinspiration as tools for the design of innovative materials and systems", *Nat. Mater.*, **4**(4), 277-288. https://doi.org/10.1038/nmat1339.

Sayer, M., Bektaş, N.B. and Sayman, O. (2010), "An experimental investigation on the impact behavior of hybrid composite plates", *Compos. Struct.*, **92**(5), 1256-1262. https://doi.org/10.1016/j.compstruct.2009.10.036.

Seifoori, S., Izadi, R., Liaghat, G.H. and Parrany, A.M. (2021), "An experimental study on damage intensity in composite plates subjected to low-velocity impacts", *Polym. Test.*, **93**, 106887. https://doi.org/10.1016/j.polymertesting.2020.106887.

Shi, Y., Pinna, C. and Soutis, C. (2020), "Impact damage characteristics of carbon fibre metal laminates: experiments and simulation", *Appl. Compos. Mater.*, **27**, 511-531. https://doi.org/10.1007/s10443-020-09800-y.

Tay, T. (2003), "Characterization and analysis of delamination fracture in composites: an overview of developments from 1990 to 2001", *Appl. Mech. Rev.*, **56**(1), 1-32. https://doi.org/10.1115/1.1504848.

Tay, T.E., Liu, G., Tan, V.B.C., Sun, X.S. and Pham, D.C. (2008), "Progressive failure analysis of composites", *J. Compos. Mater.*, **42**(18), 1921-1966. https://doi.org/10.1177/0021998308093912.

Thomason, J.L. and Rudeiros-Fernández, J.L. (2018), "A review of the impact performance of natural fiber thermoplastic composites", *Front. Mater.*, **5**, 60. https://doi.org/10.3389/fmats.2018.00060.

Wade, B., Feraboli, P. and Osborne, M. (2012), "Simulating laminated composites using LS-DYNA material model MAT54 Part I: [0] and [90] ply single-element investigation", FAA JAMS, Baltimore, MD, USA.

Wang, H., Wang, C., Hazell, P. J., Wright, A., Zhang, Z., Lan, X., ... & Zhou, M. (2021), "Insights into the high-velocity impact behaviour of bio-inspired composite laminates with helicoidal lay-ups", *Polym. Test.*, **103**, 107348.

Wisnom, M.R. (2010), "Modelling discrete failures in composites with interface elements", *Compos. Part A: Appl. Sci. Manuf.*, **41**(7), 795-805. https://doi.org/10.1016/j.compositesa.2010.02.011.

Ying, S., Mengyun, T., Zhijun, R., Baohui, S. and Li, C. (2017), "An experimental investigation on the low-velocity impact response of carbon-aramid/epoxy hybrid composite laminates", *J. Reinf. Plast. Compos.*, **36**(6), 422-434. https://doi.org/10.1177/0731684416680893.

Zhang, C., Li, N., Wang, W., Binienda, W.K. and Fang, H. (2015), "Progressive damage simulation of triaxially braided composite using a 3D meso-scale finite element model", *Compos. Struct.*, **125**, 104-116. https://doi.org/10.1016/j.compstruct.2015.01.034.

Zhang, J. and Zhang, X. (2015), "An efficient approach for predicting low-velocity impact force and damage in composite laminates", *Compos. Struct.*, **130**, 85-94. https://doi.org/10.1016/j.compstruct.2015.04.023.

Zhang, J. and Zhang, X. (2015), "Simulating low-velocity impact induced delamination in composites by a quasi-static load model with surface-based cohesive contact", *Compos. Struct.*, **125**, 51-57. https://doi.org/10.1016/j.compstruct.2015.01.050.

Zhang, Y., Zhu, P. and Lai, X. (2006), "Finite element analysis of low-velocity impact damage in composite laminated plates", *Mater. Des.*, **27**(6), 513-519. https://doi.org/10.1016/j.matdes.2004.11.014.

Zhou, G., Sun, Q., Chen, Z., Zeng, D. and Su, X. (2018), "Experiment and simulation study on unidirectional carbon fiber composite component under dynamic three-point bending loading", *SAE Int. J. Mater. Manuf.*, **11**(4), 499-504.

CC